A compact size multiband printed monopole antenna with triple sense circular polarization for wireless applications

M. AL-MIHRAB[a], A. SALIM[b], H. AL-SAEDI[c], J. ALI[b]
[a]*Department of Electronic and Communication Engineering, Cankaya University, Eskisehir Yolu 29. km, Etimesgut, Ankara, 06790, Turkey*
[b]*Microwave Research Group, Department of Electrical Engineering, University of Technology, Baghdad, Iraq*
[c]*Centre of intelligence antenna and Radio systems, Department of Electrical and Computer Engineering, University of Waterloo, Waterloo, Canada*

A penta-band printed monopole antenna based on a hexagonal open loop shape is presented in this paper. The proposed antenna demonstrated a variety in the polarization. Antenna is loaded with some parts and two stair-shaped slits is created in the partial ground plane for enhancing the multiband behavior. A circularly polarized (CP) waves are generated at a three bands with impedance bandwidths (IBWs) of 10.62%, 33.65% and 8.61% centered at 1.60, 5.20 and 6.50 GHz and 3-dB axial ratio bandwidths (ARBWs) of 9.10%, 7.58%, and 4.41% respectively. While a linearly polarized (LP) waves at the other two bands over ranges (2.51-2.64 GHz) and (3.10-3.31 GHz). Besides, the proposed antenna showed a different sense of circular polarization; right hand, left hand, and right hand. The antenna is simulated and fabricated on an FR-4 (glass epoxy) substrate with relative permittivity of 4.6, thickness of 1.6 mm and a loss tangent of 0.02. The properties of multiband and circular polarization, makes the proposed antenna candidates for many modern wireless applications.

(Received September 15, 2019; accepted October 22, 2020)

Keywords: Multiband antenna, Circular polarization, Printed antenna, Triple sense, Axial ratio

1. Introduction

Recently, wireless communication technology has been developed strikingly due to the common view of the world, which goes towards mobilized and low-cost technology. A multiple frequency band antenna is seen as one of the ultimate solutions to cover this rapid development in modern wireless communication systems [1-7]. Accordingly, circularly polarized (CP) and linearly polarized (LP) printed antennas have attained profusely in modern wireless technologies. A monopole antenna inherently is an LP antenna. The CP waves possess better efficiency as compared with LP waves in global navigation satellite systems (GNSS) because CP waves are impregnable to the errors resulted from polarization rotation and ionospheric variations [8]. Several methods with variety of antennas shapes and feeding methods are introduced for realizing a wideband or multiband CP antennas [9-26]. In [9], the ground plane is modified with a hook-shaped branch and fed by an inverted asymmetric arm L-shaped microstrip line for a wide band CP antenna.

A sickle-shaped radiator with a circular slotted ground plane and tapered feed line is introduced in [10] for the wideband CP.

In [11], two truncated square slit patches are stacked with capacitive feed. In [12], three truncated and slot patches are stacked with artificial meta-surface for improving antenna radiation efficiency for triple band GPS frequencies L1, L2 and L5. GNSS antenna is demonstrated in [13, 14]; it consists of multi annular [13] and square [14] stacked patches fed by multiport. In [15-17], a cavity-backed reflector with a crossed dipole is used to construct multiband CP antennas with a unidirectional radiation pattern. In [15], double-sided printed crossed dipoles are used with vacant quarter printed rings are loaded with complementary split ring resonators (CSRRs) to generate dual band CP while LC resonators are employed [16] instead of CSRRs to obtain three CP bands. In [17], two unit cells of a via less composite right/ left-handed transmission line are loaded on the arms of a reference double-sided printed dipole to implement triple band CP. In [18, 19], fractal geometry is employed to obtain multiband CP. In relating to [18], two fractal types (Koch and Minkowski) are implemented at the end of a square patch and etched a 45° rotated poly fractal slot in the center for multiband CP operation. In [19], a Koch fractal is fulfilled to a rectangular patch with a crossed slot at the center and excited by a coplanar waveguide (CPW). Also, single layer designs achieved by using square, hexagonal, and annular slots on the ground with an appropriate radiator that have been demonstrated in [20-24]. In [25], a triple band CP is realized by a patch antenna consists of a tilted inverted-U-shaped radiator with extra I and L shaped strips as well as a partial ground plane. A Y-shaped

monopole antenna with L-shaped slot loaded on the ground plane is presented in [26] to build a triple CP band.

In this paper, a triple CP band, as well as a double LP band, has been obtained by a new structure printed antenna with an open-loop hexagonal radiator. The proposed antenna has an overall size of $65\times45\ mm^2$ which corresponds to $0.33\lambda_\circ \times 0.23\lambda_\circ$. This antenna can be utilized in GNSS, C-band applications as a CP and Broadband Radio Service (BRS), IEEE 802.16e (Mobile WiMAX), Long-Term Evolution (LTE) and Radiolocation Service such as Radars as a LP. All simulation results in this paper are obtained by the use of software ANSYS HFSS13.0.0.

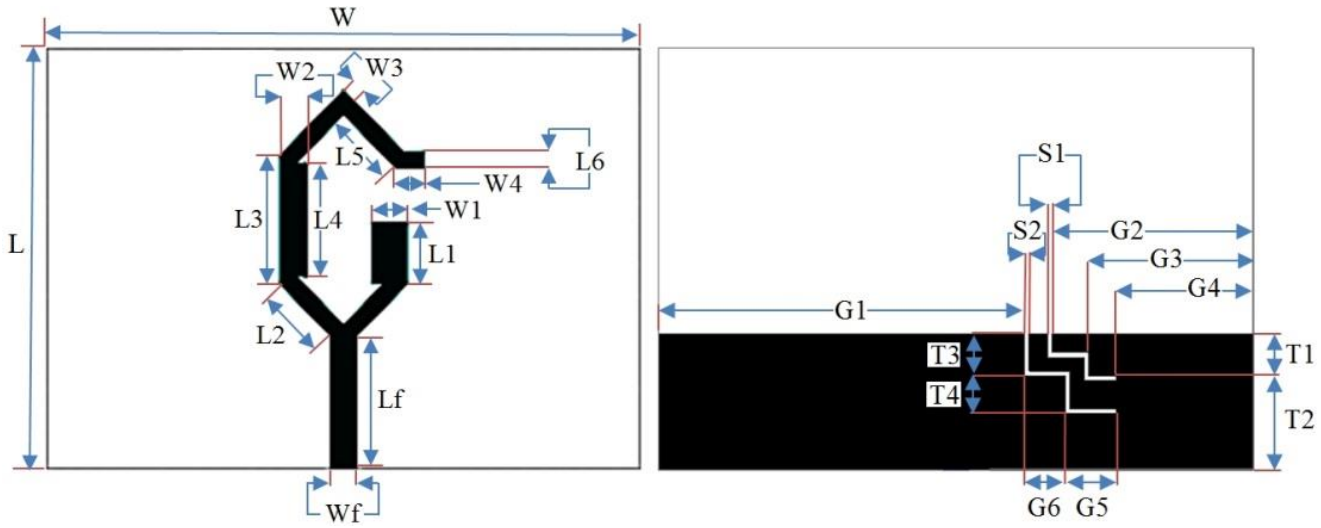

(a) *(b)*

Fig. 1. Configuration of the proposed antenna: (a) top view (b) bottom view (color online)

2. Antenna design and analysis

2.1. Antenna configuration

The structure of the proposed antenna is illustrated in Fig. 1. It is printed on an FR-4 (glass epoxy) substrate which has a thickness of 1.6 mm with a relative permittivity of $\varepsilon_r = 4.4$ and a loss tangent of $\tan\delta = 0.02$. An open loop radiator in the form of a hexagonal shape is printed on the upper surface of the substrate while the partial ground plane with double slit stairs settled on the rear side of the substrate. The antenna is fed via a 50Ω microstrip transmission line. The radiator occupies an area of $0.14\lambda_\circ \times 0.08\lambda_\circ$. An intensive full-wave simulation has been performed to optimize the proposed antenna parameters that are listed in Table 1.

2.2. Design procedure

The design evolution of the proposed antenna is demonstrated in Fig. 2. Initially, the radiator part is a closed loop hexagonal ring, as shown in Ant.1of Fig. 2. It supplies two operating bands from (2.05-2.41 GHz) and (5.50-6.75 GHz) as illustrated in Fig. 3(a); however, the resultant antenna generates elliptical polarization at the operating frequencies, as shown in Fig. 3(b). In Ant.2, the operating bands shifted towards lower frequency (1.61-1.75 GHz). Further, the second band is extended over the frequency range (2.95-5.45 GHz), as shown in Fig. e 3 (a). Also, the AR is improved as compared with Ant.1 and becomes less than 3-dB as presented in Fig. 4, but the second AR band is not overlapped with the magnitude of impedance band. The ranges of the operating frequency increased in the Ant.3 by adding loading parts to the radiator, the operating bands became (1.60-1.70 GHz), (2.93-3.42 GHz) and (4.10-6.61 GHz) but the circular polarization condition is verified from (1.73-1.80 GHz) which is not matching with the first operating band at Ant.3. In Ant.4 (final design), five operating bands have been realized, but AR results indicate that only three bands (1.60-1.75 GHz), (4.54-4.90 GHz) and (6.21-6.49 GHz) satisfy the CP condition. So, the concentration will be only on these three bands.

Table 1. Parameters of the proposed antenna

Parameter	Unit (mm)	Parameter	Unit (mm)	Parameter	Unit (mm)
W	45	L3	13.757	T3	4.5
W1	4.071	L4	12.242	T4	4.5
W2	3.071	L5	8	G1	40
W3	2	L6	1.914	G2	22
W4	3.343	Lf	14.421	G3	18
Wf	3	S1	0.5	G4	15
L	65	S2	0.5	G5	5.5
L1	6.757	T1	4.5	G6	4.5
L2	7.525	T2	10		

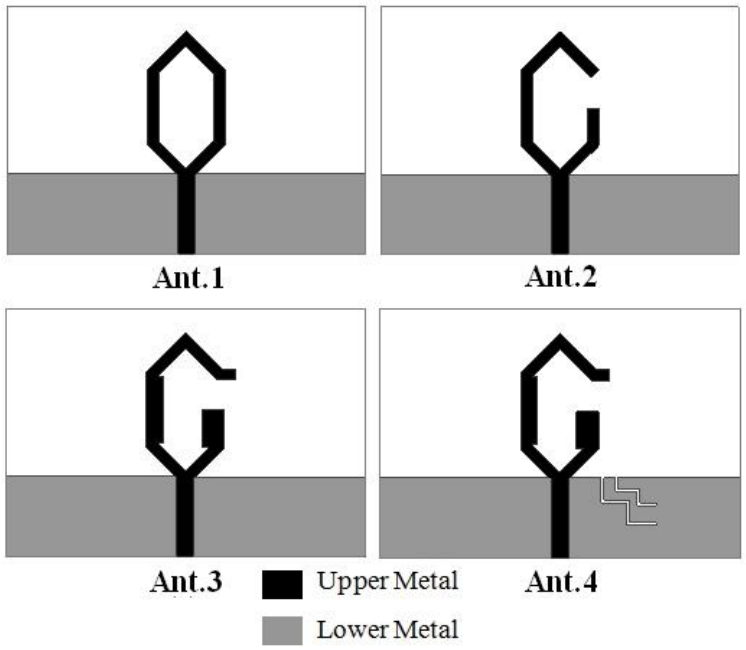

Fig. 2. Steps of the proposed antenna design

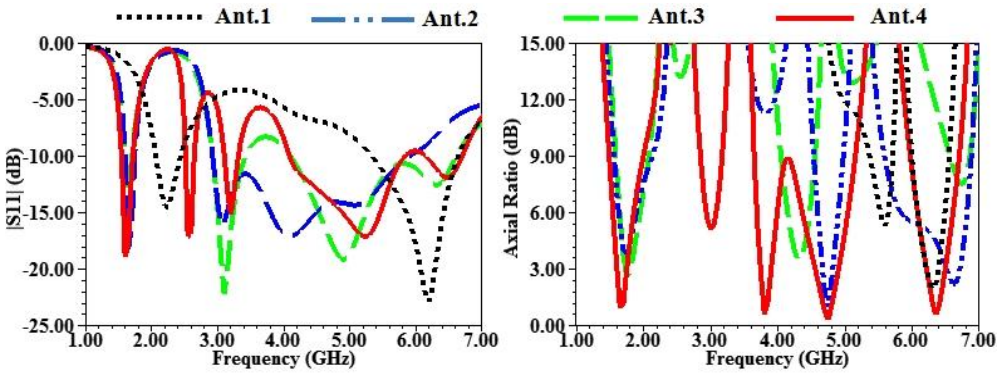

(a) (b)

Fig. 3. |S11| and Axial Ratio comparison for different configurations of Fig. 2 (color online)

2.3. Surface current distribution

To fully understand the operating mechanism of the proposed antenna, its current distributions at three resonant frequencies 1.60, 5.25, and 6.50 GHz is presented in Fig. 4 (a), (b), and (c).

In Fig. 4(a), and (b), the surface current is reinforced on the open loop hexagonal radiator specifically in the lower part of the radiator; whereas, the surface current at the third CP operating frequency concentrated in the middle and upper part of the radiator. Regarding the surface current distribution in the partial ground plane, it

intensified around the two stairs-shaped slits which contribute efficiently to increase the matching of the first operation band and to generate the 3rd CP operation band as shown in Fig. 3.

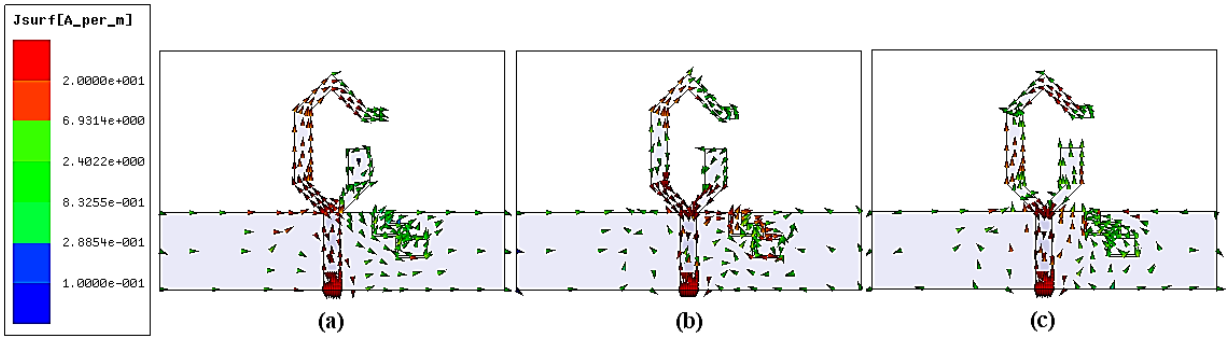

Fig. 4. The surface current distribution of the proposed open hexagonal ring printed antenna at CP bands: (a) 1.60 GHz (b) 5.25 GHz and (c) 6.50 GHz resonance frequencies (color online)

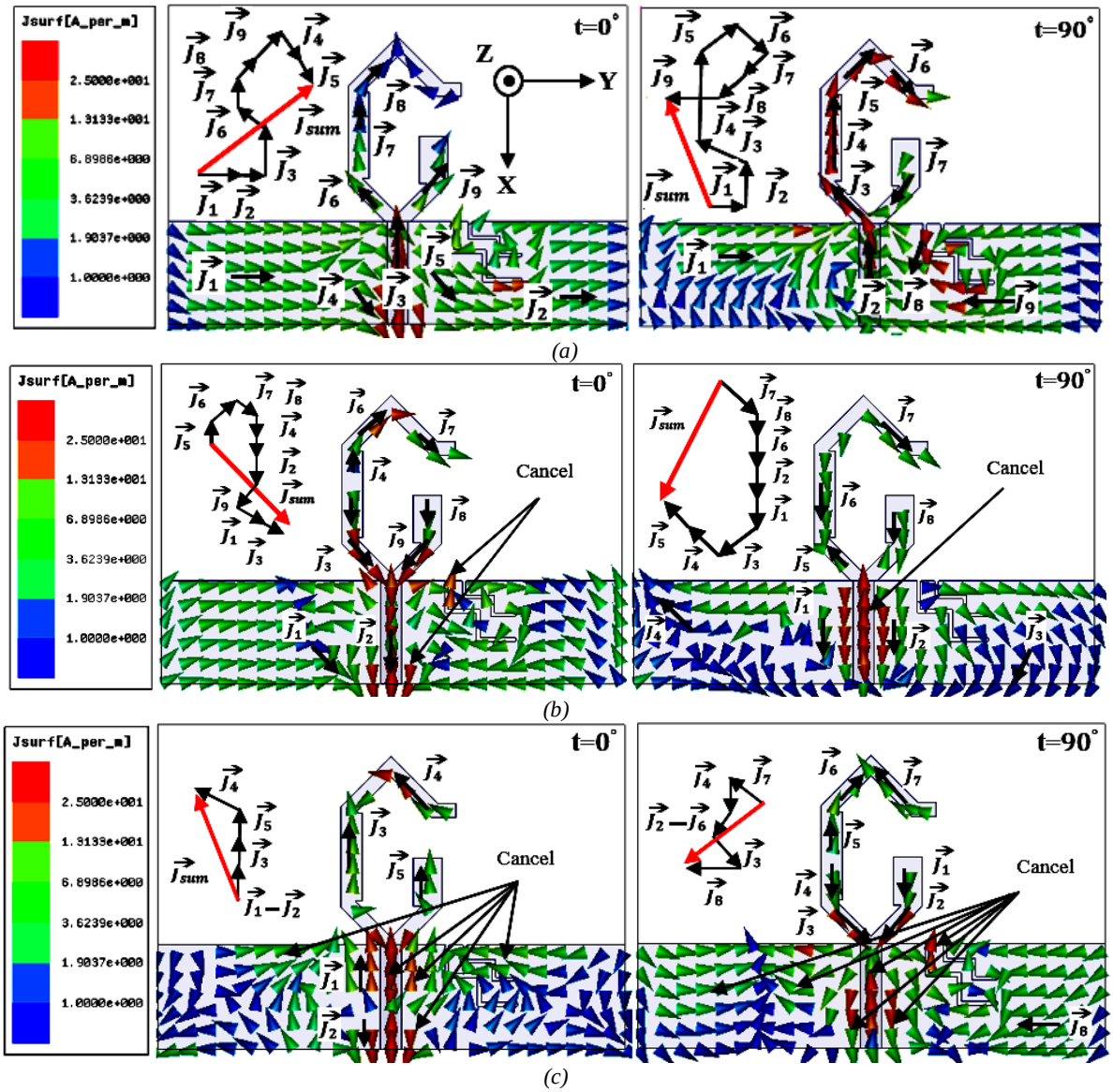

Fig. 5. The surface current distribution of proposed open hexagonal ring printed antenna at (a) 1.65 GHz (b) 4.75 GHz and (c) 6.35 GHz CP center frequencies (color online)

To study the characteristics of the CP of bands precisely, the surface current distributions plotted at 1.65, 4.75 and 6.35 GHz with time instants 0° and 90° as shown in Fig. 5. It can be noted that the CP radiation about at 1.65 GHz was obtained because of identical amplitudes and nearly 90° phase difference on the open-loop hexagonal radiator and partial ground plane, especially in the region of the double slit. Likewise, the CP radiation at about 4.75 GHz and 6.35 GHz appeared due to distributed current in open-loop hexagonal monopole especially in upper and lower arms, embedded double slits, and the partial ground plane.

From Fig. 5 (a), (b), and (c), it can be comprehended that at time instants 0° and 90°, the resultant current vector (Jsum) rotates anticlockwise direction leads to contribute right-handed circular polarization (RHCP) radiation in the +z-direction. While in Fig. 5(b), it noted that the resultant current vector rotates clockwise direction leads to contribute left-handed circular polarization (LHCP) in the +z-direction. As a consequence, it can be deduced that at 1.65 GHz and 6.35 GHz, the antenna radiates RHCP wave whereas, at 4.75 GHz, it radiates LHCP wave. Currents with opposite directions and equal magnitudes cannot contribute to identify the main direction of currents rotation. Therefore, it can be canceled.

2.4. Parametric study

To study the effects of different parameters of the suggested antenna on all operated bands and CP, parametric studies have been conducted to show such effects on the reflection coefficient |S11| and the AR for different values of W1, W2, W4, L1, S1 and S2 have been expressed. The study is implemented to each parameter independently so as to demonstrate each parameter on the behavior of multiband CP antenna.

2.4.1 The effect of W1

The impact of w1 which acts the width of the open ended rib on the magnitude of the input reflection coefficient |S11| and AR of antenna appeared evident through Fig. 6(a), and (b). As can be shown from Fig. 6(a), the influence of increasing W1 step by step towards to inner lead to the appearance of third CP operation frequency from (6.14-6.70 GHz) and CP achieved from (6.21-6.49 GHz) as illustrated in Fig. 6(b). Meanwhile, the CP region on the second band shifted towards the left side to be making more matching with the |S11|.

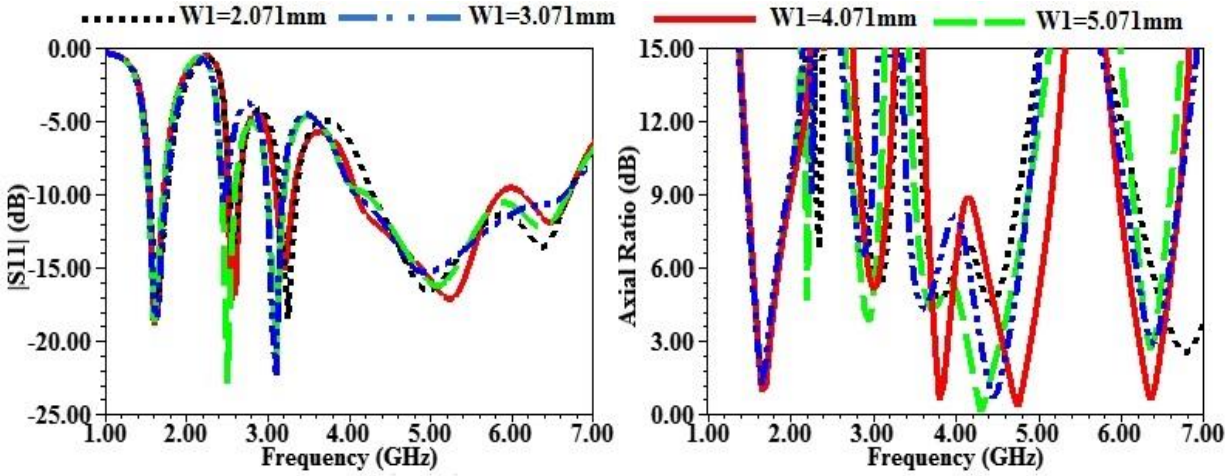

(a) *(b)*

Fig. 6. The effect of W1on the antenna performance: (a) |S11| (b) AR (color online)

2.4.2 The effect of W2

The impact of W2, which represents the width of long rib on the radiator in |S11| and AR on multiband CP antenna behavior, is presented in Fig. 7(a), and (b), respectively. Fig. 7(a), and (b), reveals the influence of W2 on over all bands, specifically for wide part (4-7 GHz). When W2=2.071mm, the reflection coefficient is weak in all band as well as the CP presents in the first band only. The increasing of W2 slightly leads to the appearance of second and third CP bands with AR less than 3-dB. Hence, the W2=3.071 mm selected as per this study. When W2 is increased, the optimum value, it affects directly to the third CP band as well as the second CP band shifted to unwanted region as seen in Fig. 7 (b).

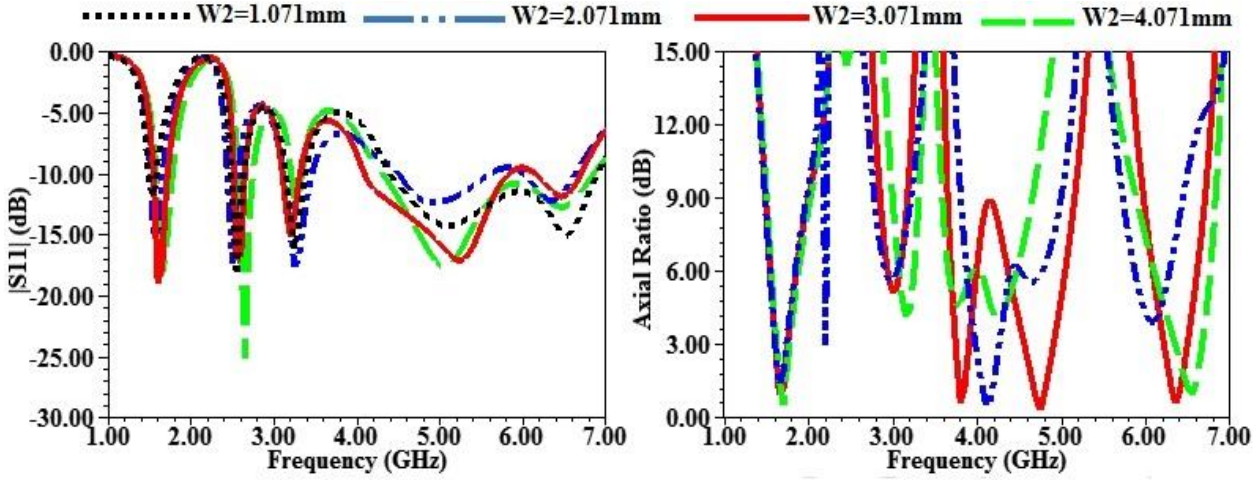

(a) *(b)*

Fig. 7. The effect of W2 on antenna performance: (a) |S11| (b) AR (color online)

2.4.3 The effect of W4

From Fig. 8, the effect of W4 which expresses a width of external loaded part connected with the end of open side rib to first operation band is unfavorable for somewhat while it plays an important role regarding the other operation bands. When w4 increased step by step, the third CP band start to appear gradually, as illustrated in Fig. 8(a), but this appearance must be compared with AR. When W4= 3.343 mm, the AR matched with |S11| at (6.21-6.49 GHz) as seen in Fig. 8(a), and (b).

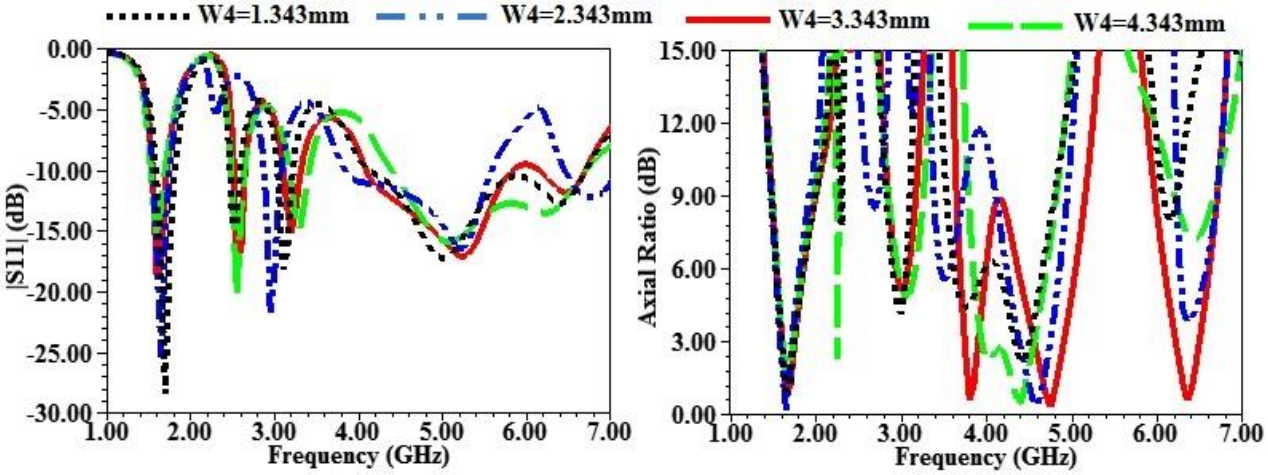

(a) *(b)*

Fig. 8. The effect of W4 on antenna performance: (a) |S11| (b) AR (color online)

2.4.4 The effect of L1

The L1 acts length of reduced rib in the radiator impacted directly to CP performance as seen in Fig. 9(b), while the reflection coefficient is not affected in an extreme manner as seen in Fig. 9(a). When L1= 6.757 mm the CP feature appear clearly and constitutes second and third bands.

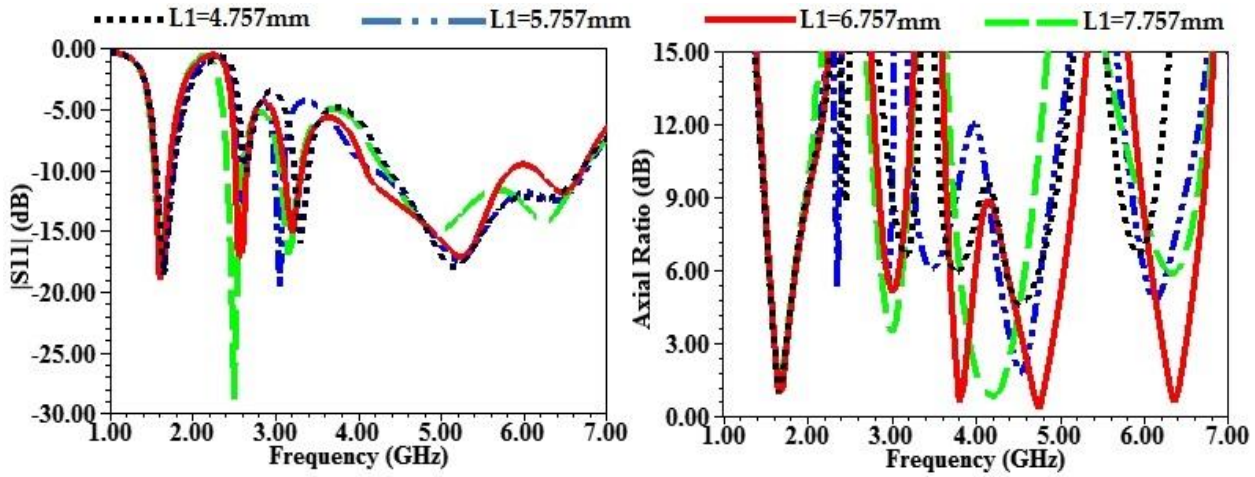

(a) *(b)*

Fig. 9. The effect of L1 on antenna performance: (a) |S11| (b) AR (color online)

2.4.5 The effect of S1 and S2

The effect of S1 and S2 in |S11| and AR on proposed antenna behavior is depicted in Fig. 10(a), and (b). The parameters S1 and S2 represent the width of the inserted slits. Increasing both of them, lead to raise the amount of matching especially at frequencies 1.65 GHz, 2.55 GHz, 3.20 GHz at the same time value of AR goes to be lower than (3dB) especially at 2nd and 3rd bands.

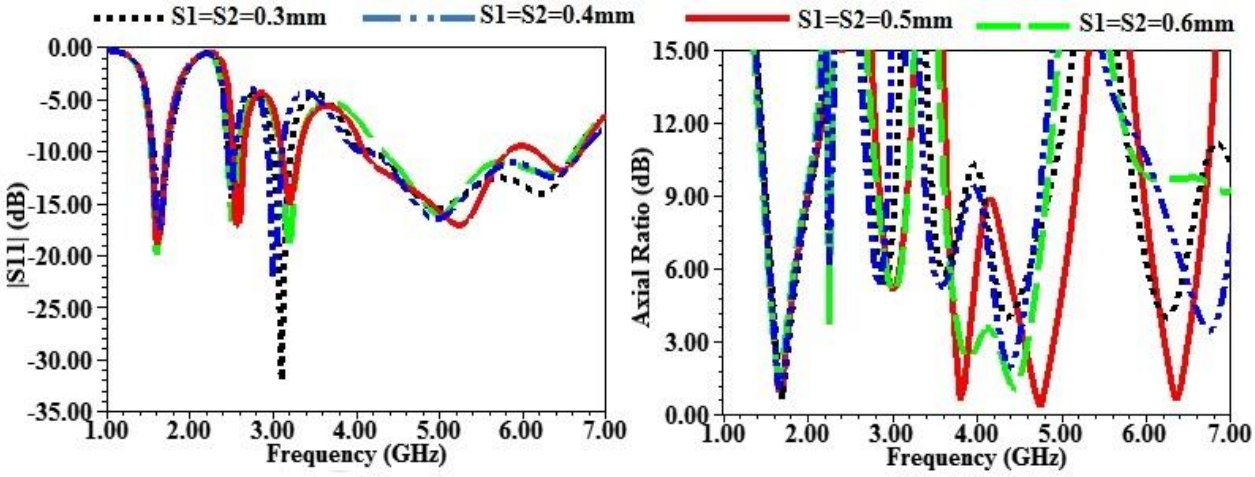

(a) *(b)*

Fig. 10. The effect of S1and S2 on antenna performance: (a) |S11| (b) AR (color online)

2.4.6 The effect of presence or not of S1 and S2

As per of Fig. 11(a), and (b), the S2 slit has considered a cornerstone of all antenna bands. When it's zero, the input reflection coefficient will increase in the first band as well as the CP condition in first band be weak and in another two bands is disappeared entirely while the s1 confined on third band performance as shown in Fig. 11(a), and (b). Therefore, the double slit S1 and S2 selected after the precise research.

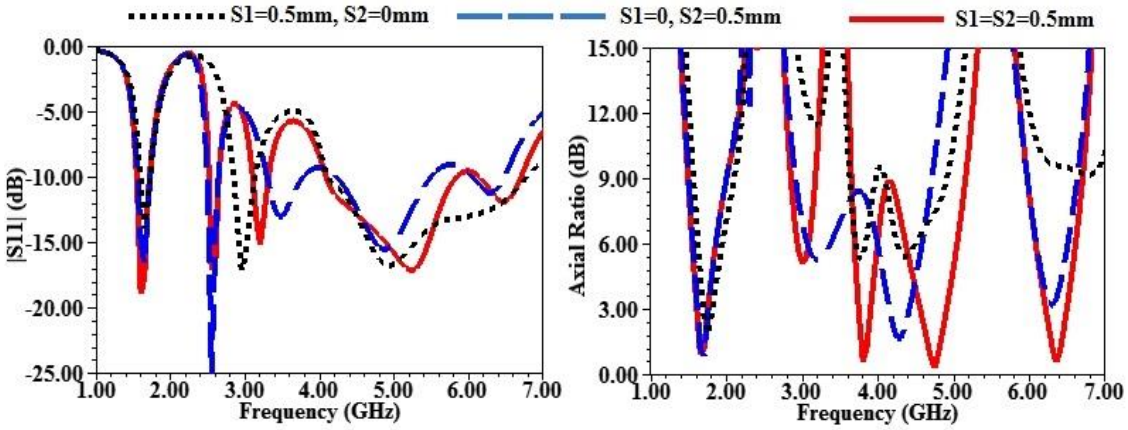

(a) *(b)*

Fig. 11. The effect of the presence or not of S1 and S2: (a) |S11| (b) AR (color online

3. Results and discussions

3.1. Reflection coefficient and ARBW

The proposed antenna parameters after optimization are illustrated in Fig. 1. Depending on these parameters, the antenna is fabricated as shown in Fig. 12 (a), (b) and measured by VNA (vector network analyzer) model (Anritsu, 3650 A) as seen in Fig.12 (c).

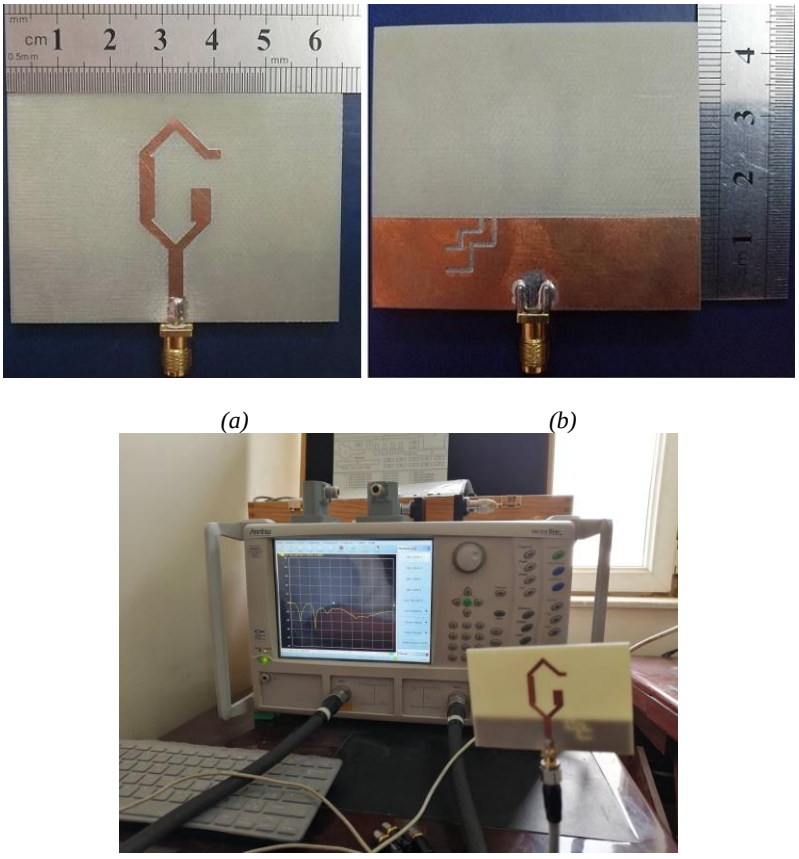

(a) *(b)*

(c)

Fig. 12. Manufactured antenna prototype: (a) top view (b) bottom view (c) during the measurement (color online)

The comparison between simulated and measured input reflection coefficient behavior can be noted in Fig. 13. The experimental result has a good matching in first two bands as well as they are comparable with the first two simulated bands approximately whereas the third band has a very poor matching under -10 dB. Regarding the identification between 4th and 5th band, it noted that practical result shifted about 500 MHz and start from 4.66 GHz to 6.51 GHz. The cause of shifting may be back to inaccuracy during the fabrication, especially the load parts in the radiator.

Regarding to ARBWs, the results between simulated and measured are identical for somewhat as shown in Fig. 13. The CP bands appear clearly in three regions. The simulated results are (1.60-1.75 GHz), (4.54-4.90 GHz) and (6.21-6.49 GHz) whilst measured results are (1.59-1.73 GHz), (4.58-4.93 GHz) and (6.25-6.50 GHz).

Concerning to two bands (2.51-2.64 GHz) and (3.10-3.31 GHz) are go to LP. As for the region from (3.74-3.90 GHz), the AR is under 3-dB but the S11>-10 dB, for this reason, it's neglected.

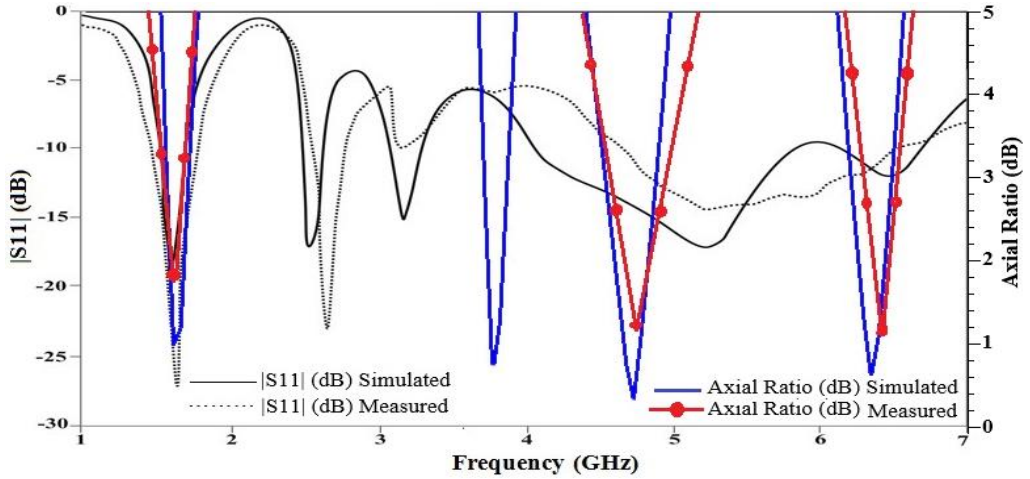

Fig. 13. Simulated and measured |S11| and Axial Ratio of the proposed antenna (color online)

3.2. Gain, radiation efficiency, and radiation pattern

The gain and radiation pattern of the proposed antenna are demonstrated in Fig. 14 and Fig. 15, respectively. From Fig. 14, it observed that the simulated and measured are comparable. The simulated peak gains are 1.87 dBi, 3.83 dBi, 3.2 dBi, 5.95 dBi and 7.67 dBi whereas the measured are1.75 dBi, 3.72 dBi, 3.2 dBi, 5.87dBi and 7.61 dBi for operating frequencies 1.65 GHz, 2.55 GHz, 3.20 GHz, 4.75 GHz and 6.35 GHz respectively. The simulated radiation efficiency of the proposed antenna is presented in Fig. 15. Based on it, the efficiency of five bands are more that 80% which gives a good indication that the antenna has high efficiency.

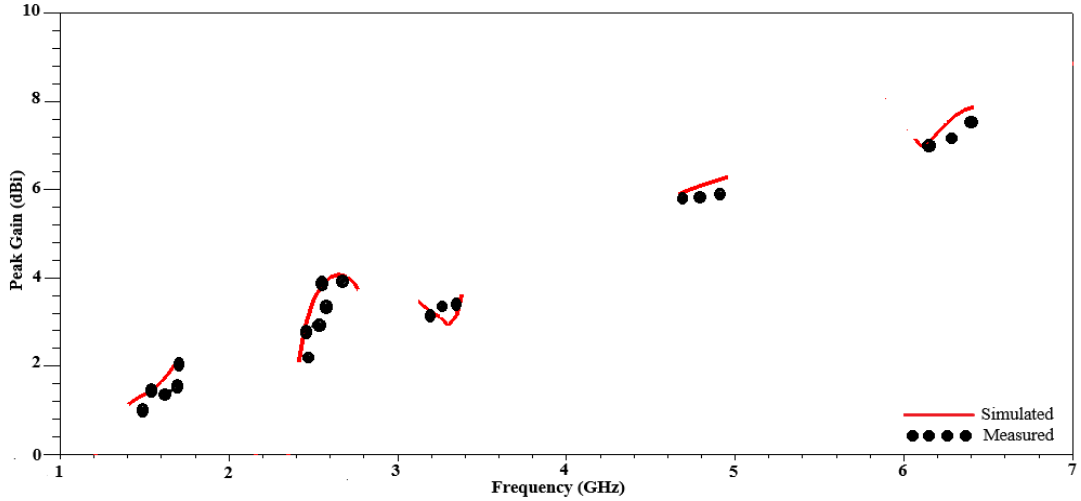

Fig. 14. Peak gain versus frequency of the proposed antenna (color online)

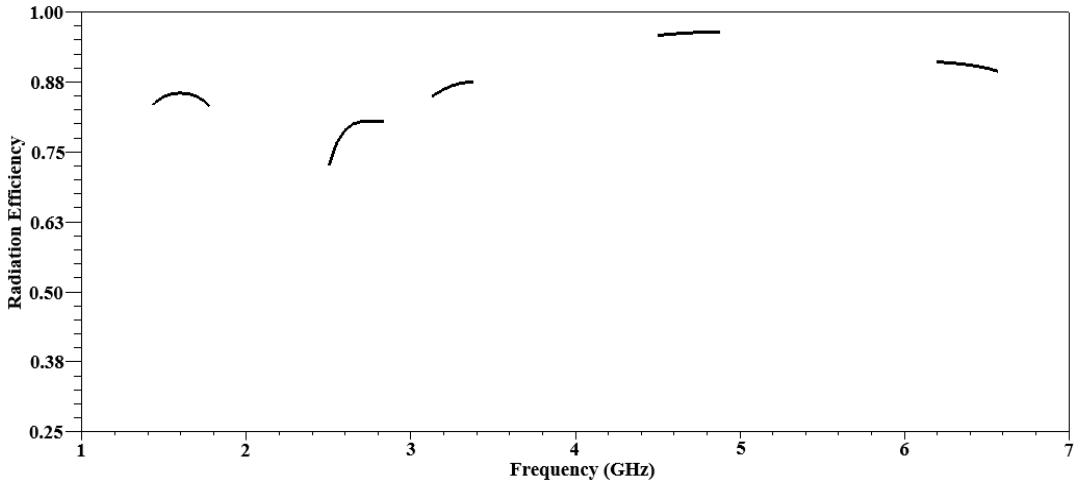

Fig. 15. Radiation efficiency versus frequency of the proposed antenna

Fig. 16(a), (b), (c), (d), and (e), demonstrates the simulated and measured normalized radiation pattern at frequencies 1.65 GHz, 2.55 GHz, 3.20 GHz, 4.75 GHz and 6.35 GHz in the XZ-plane and YZ-plane respectively. Basically, the measured results are harmony with simulated results. From Fig. 16(a), the antenna radiates RHCP wave in the + z-direction whereas LHCP wave in – z-direction. In both planes, the cross-polarization level is greater than 22 dB at $\theta = 0^{\circ}$. Also, the antenna at the 4th band (4.75 GHz) radiates LHCP wave in the +z-direction whereas RHCP in –z-direction. For final resonance frequency at 6.35 GHz, it radiates RHCP wave in the +z-direction whereas LHCP wave in the opposite direction. In the last two bands, in both of planes; the cross-polarization level is greater than 25 dB at $\theta = 0^{\circ}$.

Table 2 epitomizes the comparisons of the proposed antenna with some other previously work multiband CP antennas. During the comparison, it found that current work has many merits more than the others such as compactness, low profile, number of bands as well as carry out an enhancement in ARBW.

Table 2. Comparison of proposed work with previously published CP antennas

Ref.	**Size $\lambda_{\circ}$**	**IBW (GHz, fc, %)**	**$\|S11\| < -10$ dB Bands**	**3-dB ARBWs (GHz, fc, %)**	**3-dB ARBW Bands**	**Radiation efficiency %**	**Polarization**
[9]	0.33×0.33 ×0.0098	1.84-3.25, 1.41, 55.4	Single	1.86-3.53, 1.67, 61.96	Single	--------	LHCP
[10]	0.29×0.29 ×0.012	2.22-9.92, 7.70, 126.85	Single	2.28-4.92, 2.64, 73.33	Single	80	LHCP
[23]	0.51×0.41 ×0.0042	1.55-1.60, 1.57, 3.18 2.37-2.53, 2.40, 6.66 2.96-3.03, 3.00, 2.33	Triple	1.5275-1.5925, 1.56 2.3875-2.4725, 2.43 2.985-3.015, 3.00	Triple	--------	RHCP RHCP RHCP
[24]	0.28×0.33 ×0.0081	1.527-1.917, 1.722, 22.7 2.598-3.248, 2.923, 22.3	Dual	1.579-1.637, 1.61, 3.6 2.67-2.822, 2.74, 5.6	Dual	--------	LHCP RHCP
[26]	0.34×0.24 ×0.0084	1.57-1.85, 1.71, 16.37 1.99-2.19, 2.09, 9.56 2.52-2.77, 2.645, 9.45	Triple	1.56-1.62, 1.57, 3.70 1.98-2.08, 2.02, 4.90 2.50-2.63, 2.55, 5.06	Triple	>80	RHCP LHCP LHCP
proposed	0.33×0.23 ×0.0082	1.55-1.72, 1.60, 10.62 2.51-2.64, 2.55, 5.09 3.10-3.31, 3.20, 6.56 4.08-5.83, 5.20, 33.65 6.14-6.70, 6.50, 8.61	Penta	1.60-1.75, 1.65, 9.10 ------ ------ 4.54-4.90, 4.75, 7.58 6.21-6.49, 6.35, 4.41	Triple	85 80 87 95 90	RHCP LP LP LHCP RHCP

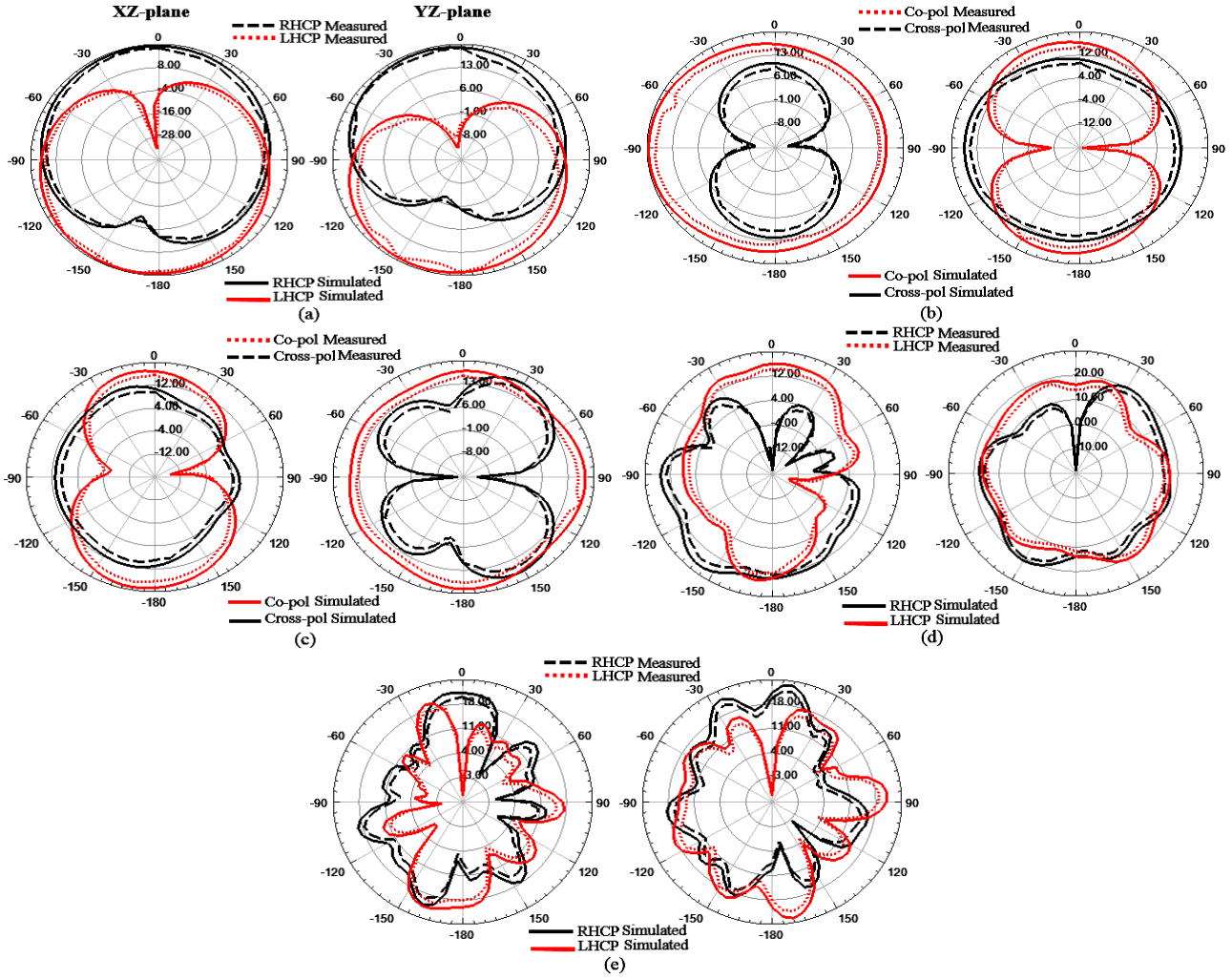

Fig. 16. Radiation patterns of the proposed open-loop hexagonal printed antenna at bands: (a) 1.65 GHz (b) 2.55 GHz (c) 3.20 GHz (d) 4.75 GHz and (e) 6.35 GHz (color online)

4. Conclusions

In this paper, an antenna with a penta-band and CP is presented. Based on the parametric study, it is noted some of the antenna design parameters played a significant role in the obtained results. It is found that the parameters like L_1 and w_1, which represent the loading parts dimensions, played a role in enhancement of four bandwidths while the parameter of stair-shaped slit length, S_2 led to release a bandwidth over frequency range of (2.51-2.64 GHz). In addition, S_1 and S_2 parameters played an important role in circular polarization enhancement in three bands (1.60-1.75 GHz), (4.54-4.90 GHz) and (6.21-6.49 GHz), whereas other two bands (2.51-2.64 GHz) and (3.10-3.31 GHz) go to the linear polarization. Based on these results, the antenna is eligible for covering a significant services such as GLONASS L1, BDS-1 L, LTE, BRS, Mobile WiMAX , and Radars.

Acknowledgments

The authors would like to express their thanks to the members of the Microwave Research Group, Department of Electrical Engineering, University of Technology, Iraq for the fruitful discussion and suggestions. The authors would also to extend their thanks to the staff of the Electronics Manufacturing Center, Ministry of Science and Technology, Iraq especially to Mr. Ali Sami, Mr. Bilal Alhashimy, Mr. Ghaleb N. Radad, and Mr. Mahmood R. Muhsen from, for their help in the measurements of the antenna prototypes.

References

[1] H. El Misilmani, M. Al-Husseini, K. Kabalan et al., Int. J. Antennas Propag. **2014**, 10 (2014).
[2] W. Hu, Y. Yin, S. Fan et al., J. Electromag. Waves Appl. **25**(14-15), 1953 (2011).
[3] A. Kaur, R. Khanna, M. Kartikeyan, Int. J. Microw. Wirel. Technol. **9**(2), 317 (2015).
[4] M. Khandelwal, B. Kanaujia, S. Dwari et al., Int. J. Microw. Wirel. Technol. **8**(6), 943 (2015).
[5] A. Kumar, V. Sankhla, J. Deegwal et al., AEU – Int. J. Electron Commun. **86**,133 (2018).

[6] C. Li, K. Wang, C. Chen, J. Electromag. Waves Appl. **25**(8-9), 1297 (2011).
[7] X. Wang, L. Sun, X. Lu et al., IEEE Trans. Antennas Propag. **65**(8), 4283 (2017).
[8] S. Shichang, Q. Luo, F. Zhu. Circularly polarized antennas, Wiley-IEEE Press, United Kingdom, 1, 2014, 1st ed.
[9] M. Samsuzzaman, M. T. Islam, Electronics Lett. **50**(15), 1043 (2014).
[10] M. Samsuzzaman, M. T. Islam, Sensors **18**(12), 4261 (2018).
[11] K. Saurav, D. Sarkar, K. Srivastava, IEEE Antennas Wirel. Propag. Lett. **14**, 52 (2015).
[12] K. Agarwal, Nasimuddin, A. Alphones, IET Microw. Antennas Propag. **8**(13), 1057 (2014).
[13] D. Singh, B. Kanaujia, S. Dwari et al., Microw. Opt. Technol. Lett. **57**(11), 2622 (2015).
[14] J. Li, H. Shi, H. Li et al., IEEE Antennas Wirel. Propag. Lett. **13**, 372 (2014).
[15] K. Wei, J. Li, L. Wang et al., Prog. Electromag. Res. C. **58**, 11(2015).
[16] K. Saurav, D. Sarkar, A. Singh et al., IEEE Trans. Antennas Propag. **63**(10), 4286 (2015).
[17] K. Saurav, D. Sarkar, Y. Singh et al., 2016 Twenty Second National Conference on Communication (NCC), IEEE (2016).
[18] V. Reddy, N. Sarma, Def. Sci. J. **65**(5), 379 (2015).
[19] R. Xu, J. Li, Y. Qi et al., IEEE Antennas Wirel. Propag. Lett. **16**,1763 (2017).
[20] B. Madhav, K. Sairam, M. Deepika et al., ARPN J. Eng. Appl. Sci. **10**(14), 5795 (2015).
[21] J. Baek, K. Hwang, IEEE Trans. Antennas Propag. **61**(9), 4831 (2013).
[22] L. Wang, Y. Guo, W. Sheng, J. Electromag. Waves Appl. **26**(11-12), 1389 (2012).
[23] L. Wang, Y. Guo, W. Sheng, J. Electromag. Waves Appl. **26**(14-15), 1820 (2012).
[24] C. Wang, J. Li, A. Zhang et al., J. Electromag. Waves Appl. **31**(9), 867 (2017).
[25] T. Hoang, T. Le, Q. Li et al., IEEE Antennas Wirel. Propag. Lett. **15**,1032 (2016).
[26] R. Singh, K. Saurav, D. Sarkar et al., Microw. Opt. Technol. Lett. **59**(2), 298 (2017).

*Corresponding author: c1582654@student.cankaya.edu.tr